Supporting Information

A Hybridization-Induced Charge-Transfer State Energy Arrangement Reduces Nonradiative Energy Loss in Organic Solar Cells

Yue Ren,[a] Ming-Yue Sui,[a] Li-Yuan Peng,[a] Ming-Yang Li,[a] Guang-Yan Sun,*[a] and Zhong-Min Su*[b]*

a. Department of Chemistry, Faculty of Science, Yanbian University, Yanji 133002, Jilin, China. E-mail: myli6@ybu.edu.cn (Ming-Yang Li) gysun@ybu.edu.cn (Guang-Yan Sun)

b. Laboratory of Theoretical and Computational Chemistry, Institute of Theoretical Chemistry, College of Chemistry, Jilin University, Changchun, 130023, China. E-mail: zmsu@nenu.edu.cn (Zhong-Min Su)

Contents

Section 1 Establishment of donor model

Considering their good convergence of frontier molecular orbital (FMO) energies to the experimental values, the donor polymer PM6 and PTB7-Th were simplified to four repeating units.

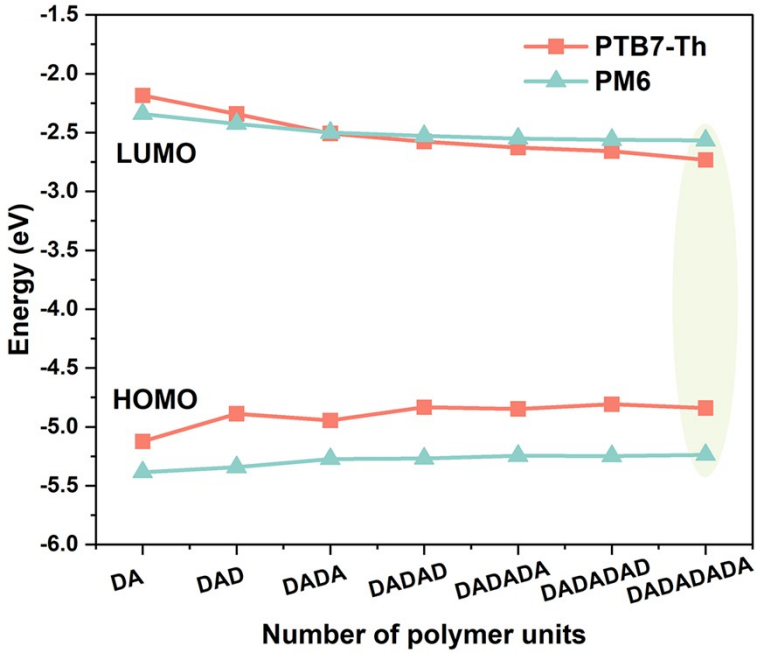

Figure S1. The evolution of molecular frontier orbital (FMO) energy levels of donor-acceptor (D-A) structural polymer donor PTB7-Th and PM6 as a function of the number of repeated units calculated at the B3LYP/6-31G(d) level.

Section 2 Molecular dynamics simulation details

The all-atom (AA) molecular dynamics (MD) simulations were performed with the GROMACS 2018.4 software package and the general AMBER force field (GAFF) with restricted electrostatic potential (RESP) charges. Consistent with the experimental weight ratios (1:1.5),[1] four donor/acceptor blends containing 25000 chlorobenzene (CB) molecules were constructs by 50 PTB7-Th polymers (each consists of four repeat units) and 187 ITIC molecules, or 178 IT-4F molecules, or 154 IEICO molecules, or 148 IEICO-4F molecules. In PM6-series (each consists of four repeat units) systems, 178 IT-4F molecules or 184 Y6 molecules were added in the blend clusters. The simulations were carried out under three-dimensional periodic boundary conditions by means of the leap-frog integrator. A spherical cut-off of 1.0 nm for summation of Van de Waals interactions and the Particle-Mesh-Ewald (PME) method for long-range Coulomb interactions were employed throughout. All processes were adopted berendsen barostat and the velocity rescaling thermostat. Each blend contained more than 340,000 atoms and was simulated by the following procedure: 1) equilibration for 10 ns under NPT ensemble to bring the solution compacted at temperature of 300 k and pressure of 1 atm; 2) employing a quasi-equilibrium approach to model the solvent evaporation processes, in which 100 solvent molecules are randomly removed every 100 ps from the solution with JAMIP software package;[2] 3) equilibration of the dried films for 50 ns after removing all solvent molecules at temperature of 300 k and pressure of 1 atm. After equilibrium, we extracted the specific snapshots of the final 1ns for further analysis.

Section 3 Nonradiative energy loss and CT-state energy

For each simulated amorphous blend film, we extracted all the donor-NFA pairs (here, a pair is defined as consisting of an adjacent polymer backbone and an NFA within a distance of ≤ 10 Å of each other) as an interfacial stacking configuration. In the presence of polarizable continuum model (PCM) with chlorobenzene, the ^{1}CT-state and ^{3}CT-state energies (where all the polymer side chains were replaced with methyl groups) were calculated by time-dependent density functional theory (TD-DFT) at the ωB97XD/6-31G(d,p) level.[3] All the above-mentioned calculations were performed in the Gaussian 16 program package.[4] Subsequently, valid CT states were identified by the natural transition orbital (NTO) analysis in Multiwfn 3.8 software package.[5] That is a significant charge transfer trajectory from donor to NFA in a pair of NTO by visualizing the distribution of holes and electrons wave functions.

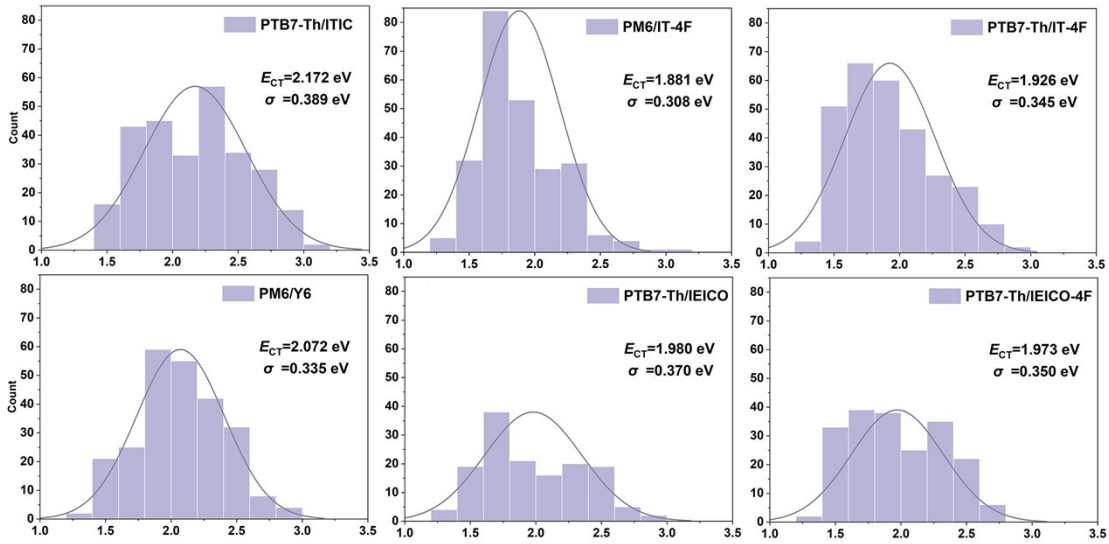

Figure S2. Distribution of charge-transfer state energies (E_{CT}) found in PTB7-Th/ITIC, PM6/IT-4F, PTB7-Th/IT-4F, PM6/Y6, PTB7-Th/IEICO and PTB7-Th/IEICO-4F blends. The darker solid lines represent Gaussian fits, which are used to extract the average E_{CT} and the standard deviation (σ).

Table S1. Experimental non-radiative energy losses (ΔE_3) and references.

	E_{CT}	ΔE_3	Ref
PTB7-Th/ITIC	2.172	0.15	6-8
PTB7-Th/IT-4F	1.926	0.39	9
PTB7-Th/IEICO	1.980	0.29	1
PTB7-Th/IEICO-4F	1.973	0.34	1
PM6/IT4F	1.881	0.34	10
PM6/Y6	2.072	0.23	10

Section 4 Hybridization of electronic states

Comparing EI region (Figure S3a) and the non-EI region (Figure S3b), the EI region shows a very obvious hybridization between the triplet excited states of donor or acceptor and ^{3}CT states (T_D/T_A and ^{3}CT). But there is no hybridization between ^{3}CT and T_1 states in the non-EI region and the hybridization between singlet excited states and ^{1}CT states is more inclined (S_D/S_A and ^{1}CT). Specifically, the ^{3}CT state is closer to the high-lying T_n state in terms of energy level in the EI region, resulting in the ^{3}CT-state energy being "lifted", and at the same time, the ^{1}CT state and the S_1 state of PTB7-Th/IT-4F have a tendency to hybridize to "pulled" down. So it presents $E_{3CT} > E_{1CT}$ finally. In the non-EI region, the ^{1}CT state of PM6/IT-4F has a very obvious hybridization with the high-lying S_n state. PTB7-Th/ITIC and PM6/Y6 are relatively complex, with the combined action of the ^{1}CT and high-lying S_n hybridization and ^{3}CT and high-lying T_n hybridization, leading $E_{1CT} > E_{3CT}$.

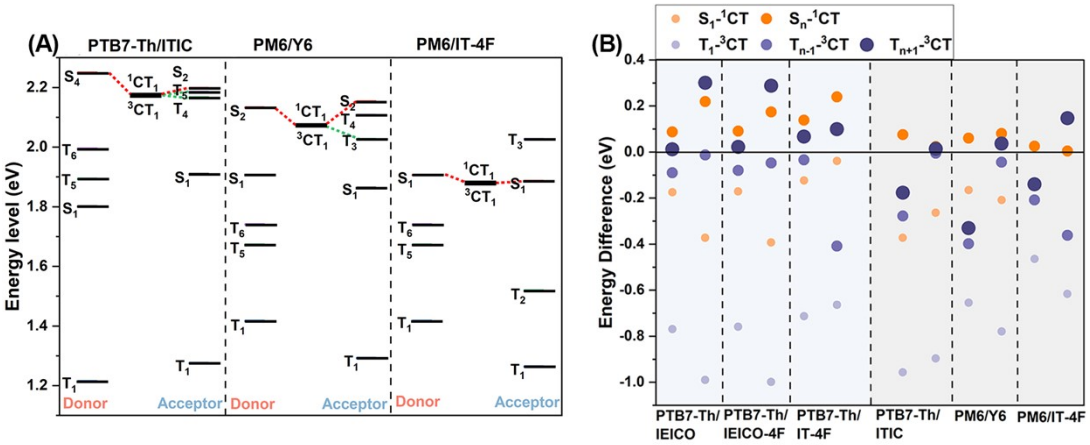

Figure S3. (a) Schematic diagram of the singlet (S_n) and triplet (T_n) excited states, and the $^1CT_1$ and $^3CT_1$ states energy levels. (b) The energy level differences between the singlet (S_n) and triplet (T_n) excited states energy levels of the donor and acceptor molecules, and the lowest singlet ($^1CT_1$) and triplet charge transfer ($^1CT_1$) states at the donor-acceptor interface.

Section 5 ^{1}CT- and ^{3}CT-state energy for all stacking configurations

We extracted all interfacial stacking configuration from MD-generated blend film. In the presence of polarize continuum model (PCM) with chlorobenzene, the ^{1}CT-state and ^{3}CT-state energies (where all the polymer side chains were replaced with methyl groups) were calculated by time-dependent density functional theory (TD-DFT) at the ωB97XD/6-31G(d,p) level in the Gaussian 16 program package. Subsequently, valid CT states were identified by the natural transition orbital (NTO) analysis in Multiwfn 3.8 software package. That is a significant charge transfer trajectory from donor to NFA in a pair of NTO by visualizing the distribution of holes and electrons wave functions. The energies of the ^{1}CT and ^{3}CT states calculated based on all the interface packing configurations in the six systems are shown in Figure S4.

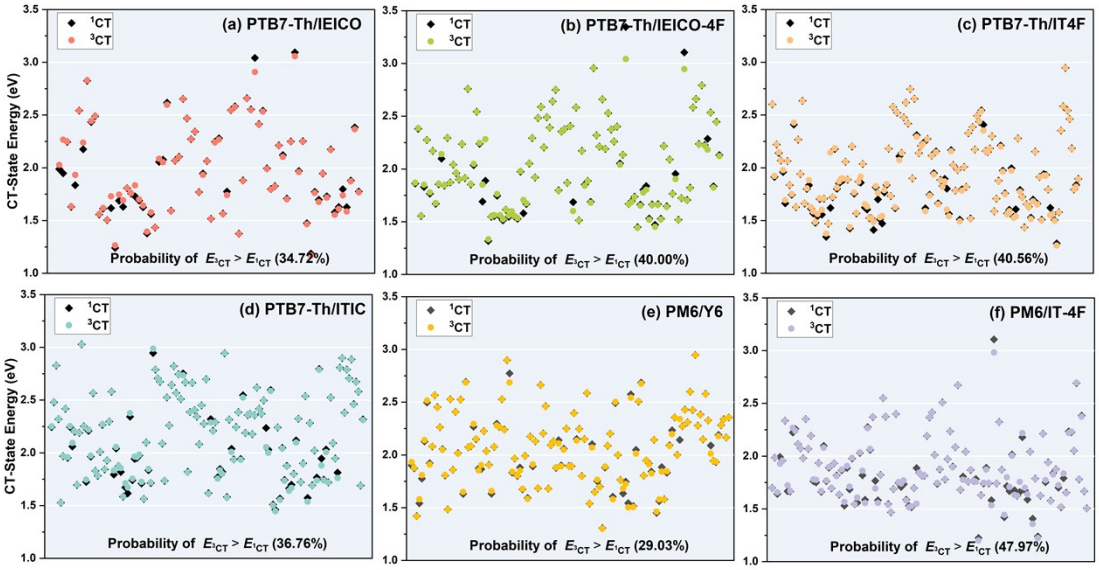

Figure S4. The energies distribution of ^{1}CT state and ^{3}CT state for all interfacial stacking configurations in (a) PTB7-Th/IEICO, (b) PTB7-Th/IEICO-4F, (c) PTB7-Th/IT-4F, (d) PTB7-Th/ITIC, (e)PM6/IT-4F, and (f) PM6/Y6 blends.

Section 6 Calculation methods of dihedral angle

We first extracted the atomic coordinates of all atoms, then divided them into distinct molecular fragments. These molecular fragments were then subjected to plane fitting using the least squares method. The error function was defined as the summation of the distances from each atom within the segment to the fitted plane. The dihedral angle between two molecular fragments was then computed as the angle between the normal vectors of the fitted planes.

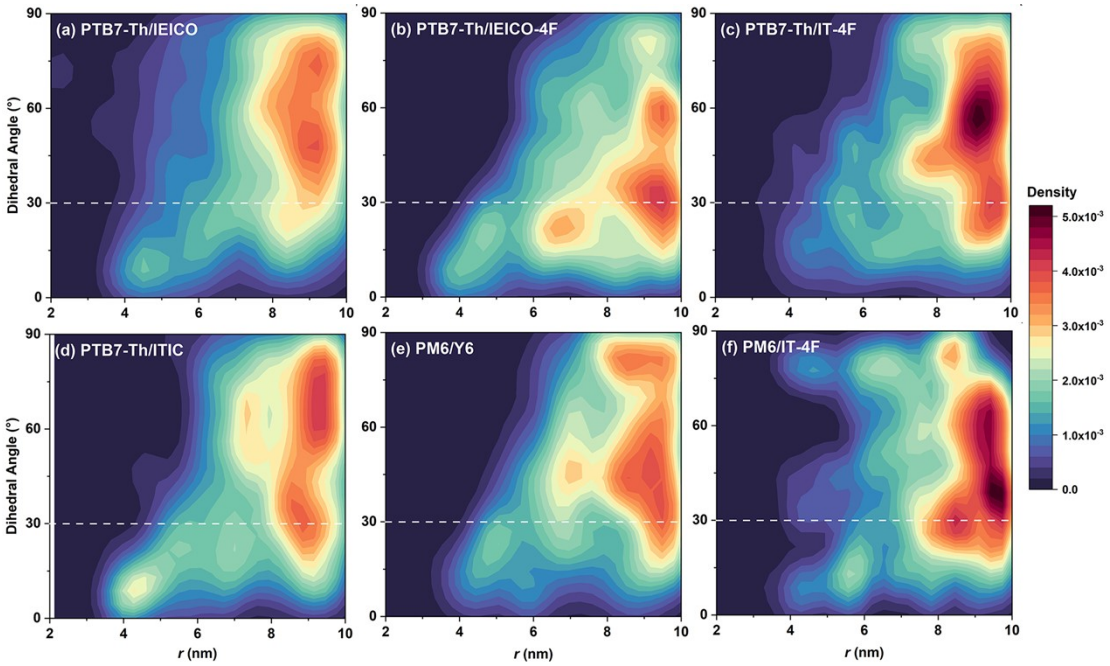

Figure S5. Density contour maps of the intermolecular centroid distance (*r*) and dihedral angles for stacking configurations. The dashed line refers to the region separated by the Face-on orientation (dihedral angle of 0°-30°). The color card corresponds to the distribution density.

Section 7 Radial distribution functions

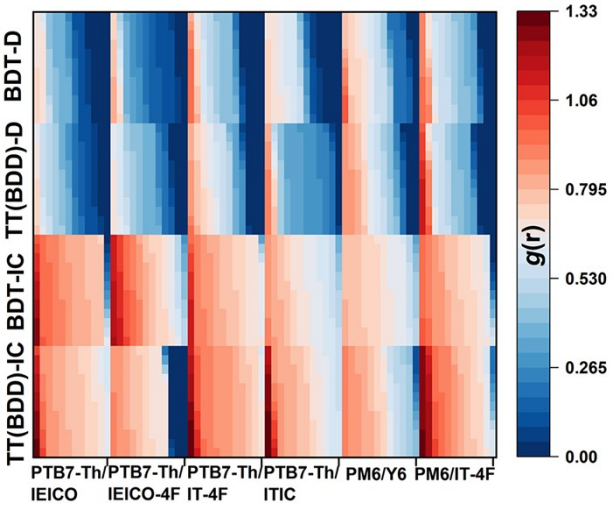

Figure S6. Radial distribution functions of BDT and TT(BDD) units relative to the IC and D units of NFAs for six MD simulated blends, and the color cards corresponding to the stacking probability *g*(r).

Section 8 Dihedral Angle between BDD or TT unit and BDT unit

As explained in Section 1, the donor polymer PM6 and PTB7-Th were simplified to four repeating units. Therefore, the dihedral angles between electron-donating and electron-withdrawing units within the four repeat units were counted in Figure S5a-d. It can be expected that the donor molecule maintains a good planarity in the film morphology, with the dihedral angle being close to 0° or 180°. There is a large torsion angle between TT unit and BDT unit in the MD simulated blend containing PTB7-Th with TT unit as donor. It indicates that the structure of PTB7-Th is deformed, which is not conducive to the formation of ordered intermolecular π-π stacking. But for PM6 with BDD and BDT unit, BDD-BDT unit maintains planarity easier by the steric hindrance provided by the large conjugated BDD-BDT units compared with TT-BDT.

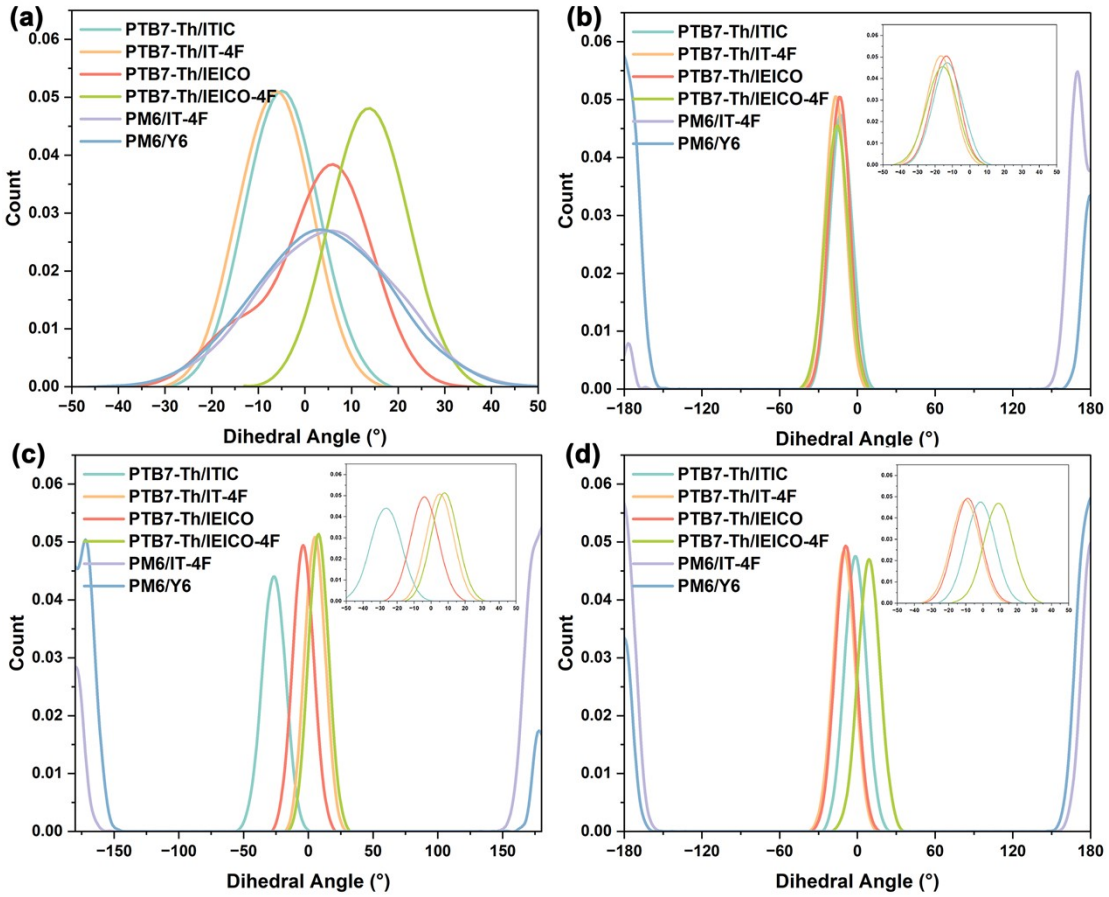

Figure S7. Distributions of dihedral angle obtained from the MD simulations. The dihedral angle of the BDD or TT unit relative to the TT unit within the four repeat cells is due to the donor including four repeat units.

Section 9 Reference

1. Karki, A.; Vollbrecht, J.; Gillett, A. J.; Selter, P.; Lee, J.; Peng, Z.; Schopp, N.; Dixon, A. L.; Schrock, M.; Nádaždy, V., et al., Unifying Charge Generation, Recombination, and Extraction in Low-Offset Non-Fullerene Acceptor Organic Solar Cells. *Adv. Funct. Mater.* **2020,** *10* (29), 2001203.
2. Zhao, X.-G.; Zhou, K.; Xing, B.; Zhao, R.; Luo, S.; Li, T.; Sun, Y.; Na, G.; Xie, J.; Yang, X., et al., JAMIP: an artificial-intelligence aided data-driven infrastructure for computational materials informatics. *Sci. Bull.* **2021,** *66* (19), 1973-1985.
3. Chai, J.-D.; Head-Gordon, M., Long-range corrected hybrid density functionals with damped atom–atom dispersion corrections. *Phys. Chem. Chem. Phys.* **2008,** *10* (44), 6615-6620.
4. Frisch, M. J.; Trucks, G. W.; Schlegel, H. B.; Scuseria, G. E.; Robb, M. A.; Cheeseman, J. R.; Scalmani, G.; Barone, V.; Petersson, G. A.; Nakatsuji, H., et al. *Gaussian 16 Rev. C.01*, Wallingford, CT, 2016.
5. Lu, T.; Chen, F., Multiwfn: A multifunctional wavefunction analyzer. *J. Comput. Chem.* **2012,** *33* (5), 580-592.
6. Shi, X.; Zuo, L.; Jo, S. B.; Gao, K.; Lin, F.; Liu, F.; Jen, A. K. Y., Design of a Highly Crystalline Low-Band Gap Fused-Ring Electron Acceptor for High-Efficiency Solar Cells with Low Energy Loss. *Chem. Mater.* **2017,** *29* (19), 8369-8376.
7. Wang, X.; Yang, Y.; He, Z.; Wu, H.; Cao, Y., Influence of the acceptor crystallinity on the open-circuit voltage in PTB7-Th: ITIC organic solar cells. *J. Mater. Chem. C* **2019,** *7* (47), 14861-14866.
8. Lin, Y.; Wang, J.; Zhang, Z.-G.; Bai, H.; Li, Y.; Zhu, D.; Zhan, X., An Electron Acceptor Challenging Fullerenes for Efficient Polymer Solar Cells. *Adv. Mater.* **2015,** *27* (7), 1170-1174.
9. Mohapatra, A. A.; Shivanna, R.; Podapangi, S.; Hinderhofer, A.; Dar, M. I.; Maity, N.; Schreiber, F.; Sadhanala, A.; Friend, R. H.; Patil, S., Role of Morphology and Förster Resonance Energy Transfer in Ternary Blend Organic Solar Cells. *ACS Appl. Energy Mater.* **2020,** *3* (12), 12025-12036.
10. Ma, L.; Zhang, S.; Zhu, J.; Wang, J.; Ren, J.; Zhang, J.; Hou, J., Completely non-fused electron acceptor with 3D-interpenetrated crystalline structure enables efficient and stable organic solar cell. *Nat. Commun.* **2021,** *12* (1), 5093.